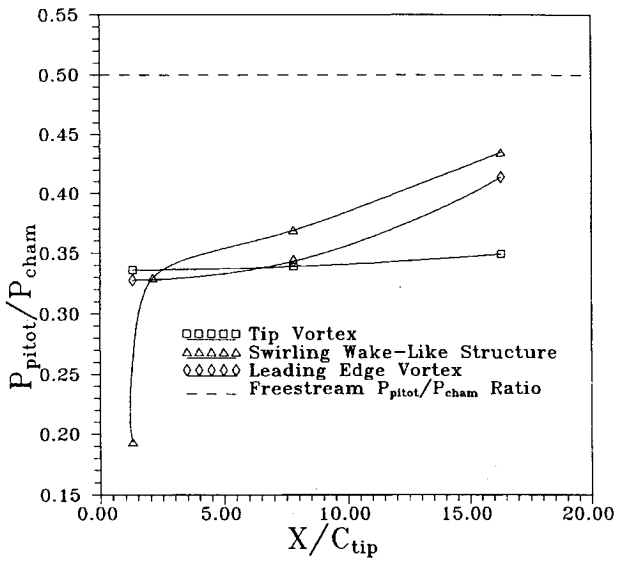

Fig. 5 Minimum pitot pressure characteristics of the three swirling structures in the vortex wake.

vortex, which itself exhibits downwash. Figure 5 summarizes the decay characteristics of the three predominant structures in the vortex wake as extracted from the pitot pressure surveys. The tip vortex and the leading-edge vortex start out at about the same pitot pressure ratio, but the latter starts relaxing towards the freestream value by $X/C_{tip} = 7.8$. The swirling wakelike structure initially has a very low pitot pressure reading but relaxes rapidly as it convects downstream. The pitot pressure readings of the tip vortex are virtually unchanged over the entire surveyed range of 16.3 tip chords, which suggests that tip vortices act as flow confinement structures that suppress diffusion. This may result in the transport of entrained passive contaminants to larger downstream distances than usual wake processes would suggest. The nature of the diffusion of these vortex flows is of concern for supersonic transport operations and may also affect the stealthiness of supersonic aircraft designs.

A rake of seven common stainless steel sewing needles with 6.35-mm spacing and pointing in the freestream direction was positioned vertically so as to lie in the plane of the three swirling structures. Shadowgraphy was used to record the Mach cones generated by the needles to provide an estimate of the axial Mach number distribution.[7,9] When the needles were placed immediately behind the model, the waves generated in the wakelike structure (feature 6) showed larger wave angles compared with those generated outside the swirling structures.[7] This qualitatively indicates that there is a wakelike axial Mach number profile in feature 6. However, when the needles were placed at the $X/C_{tip} = 2$ location, all of the waves generated by the needles appear unrefracted, and the wave angles are all essentially equivalent[7] (i.e., wave angles are within 1 deg of each other) to the freestream Mach angle.[7] Therefore, within the resolution of the photographs, the vortex wake appears to be convected downstream at the freestream Mach number very shortly after its generation. With the assumption of constant stagnation temperature in the vortex wake, the axial velocity will then be that of the freestream, suggesting that the condition of the Trefftz plane[13] is met just a short distance downstream. This implies that the application of an incompressible roll-up model[2] could be a viable approach for calculating the vortex-wake evolution from supersonic aircraft, provided that a realistic wing loading on the planform is available to initialize the subsequent vortex-wake computation.

Acknowledgments

The assistance provided by Svetozar Popovic, Michael Smart, and Lester Orlick is gratefully acknowledged.

References

[1]Anon., "In the Wake of the Concorde," *Aerospace Engineering Sciences Newsletter*, Fall 1994, p. 5.

[2]Quackenbush, T. R., Teske, M. E., and Bilanin, A. J., "Computation of Wake/Exhaust Mixing Downstream of Advanced Transport Aircraft," AIAA Paper 93-2944, July 1993.

[3]Cali, P., and Drela, M., "Implicit Euler Calculation of Supersonic Vortex Wake/Engine Plume Interaction," AIAA Paper 93-0656, Jan. 1993.

[4]Miake-Lye, R., Martinez-Sanchez, M., Brown, R., and Kolb, C., "Plume and Wake Dynamics, Mixing and Chemistry Behind an HSCT Aircraft," AIAA Paper 91-3158, Sept. 1991.

[5]Overcamp, T. J., and Fay, J. A., "Dispersion and Subsidence of the Exhaust of a Supersonic Transport in the Stratosphere," *Journal of Aircraft*, Vol. 10, No. 12, 1973, pp. 720–728.

[6]Fuhrmann, H. D., "Application of Natural Laminar Flow to a Supersonic Transport Concept," AIAA Paper 93-3467, Aug. 1993.

[7]Wang, F. Y., Sforza, P. M., and Pascali, R., "Vortex-Wake Characteristics of a High Speed Civil Transport Type Wing Planform at Mach 2.5," AIAA Paper 95-2284, June 1995.

[8]Miller, D. S., and Wood, R. M., "Leeside Flows over Delta Wings at Supersonic Speeds," *Journal of Aircraft*, Vol. 21, No. 9, 1984, pp. 680–686.

[9]Wang, F. Y., and Sforza, P. M., "An Exploratory Wind Tunnel Study of Supersonic Tip Vortices," AIAA Paper 93-2923, July 1993.

[10]Wang, F. Y., and Sforza, P. M., "An Experimental Investigation of Tip Vortices at Mach 2.5," AIAA Paper 93-3448, Aug. 1993.

[11]Smart, M. K., Kalkhoran, I. M., and Bentson, J., "Measurements of Supersonic Wing Tip Vortices," *AIAA Journal*, Vol. 33, No. 10, 1995, pp. 1761–1768.

[12]Smith, L. G., Maurice, M. S., Seibert, G. L., and Tyler, C., "Laser Velocimetry Measurements of Supersonic Vortex Flows on a Simple Razor-Edge Delta Wing," AIAA Paper 91-1684, June 1991.

[13]Sears, W. R. (ed.), *High Speed Aerodynamics and Jet Propulsion, Vol. 6: General Theory of High Speed Aerodynamics*, Princeton Univ. Press, Princeton, NJ, 1954, pp. 226–229.

Dynamic Buckling of Long Thin Elastic Plate Under Rapidly Applied Shear Loading

Emil T. Dankov*
University of Cincinnati, Cincinnati, Ohio 45221-0070

Introduction

THIN-WALLED structures are widely used in construction, shipbuilding, aircraft, spacecraft, etc. Many of their elements are, in fact, thin elastic plates. They transmit out-of-plane forces as well as in-plane (membrane) forces to the neighboring elements of the structure. That is why the buckling analysis is very important for their design. It is well known that in the classical theory of stability the loads are considered to be applied statically (i.e., gradually and slowly). But in reality the dynamic loads are predominant (they may be time dependent or time independent). There are three approaches for the analysis of the dynamic stability[1]: equations of motions approach (Budiansky–Roth), total energy-phase plane approach (Hoff–Hsu), and total potential energy approach (Hoff–Simitses). The dynamic stability of plates has been discussed by many authors,[2–5] but they considered mainly the case of compressive loading. Some of them considered also the case of shear loading,[3,5,6] but either the deflections were assumed to be small,[3] or in the case of large deflections only a rectangular plate with small difference between the sides was analyzed,[5] or in the case of a long thin elastic plate the changes in the slope of the nodal lines and in the length of the half-waves with the increase of loading were not taken into account.

Received Feb. 2, 1995; revision received Sept. 4, 1995; accepted for publication Sept. 29, 1995.

*Visiting Fulbright Scholar, Department of Aerospace Engineering and Engineering Mechanics; currently Independent Consultant, Tsar Ivan Shishman 16, Sofia 1000, Bulgaria.

That is why the subject of this Note is the analysis of dynamic buckling of long thin elastic plates under in-plane shear loading along the edges on the basis of the large-deflection theory, taking into account the changes in the slope of the nodal lines and in the length of the half-waves with the increase of loading. An ideal and isotropic plate is considered, but the analysis, employed herein, can be easily extended to anisotropic or imperfect plates.

Basic Differential Equations for the Case of Dynamic Plate Buckling

The equation of motion approach will be used for the dynamic buckling analysis. Because dynamic loadings will be considered, which at a given moment become greater than the critical loading, the large-deflection plate equations will be used to analyze the inertial effects in the postbuckling phase.

The strain-displacement relations are

$$\varepsilon_x = u_{,x} + 0.5w_{,x}^2$$
$$\varepsilon_y = u_{,y} + 0.5w_{,y}^2 \tag{1}$$
$$\gamma_{xy} = u_{,y} + v_{,x} + w_{,x}w_{,y}$$

where ε_x, ε_y, and γ_{xy} are middle surface strains; u and v are the in-plane displacements along the axes x and y, respectively; and w is the out-of-plane displacement (along axis z). (Note that the derivatives are denoted by a comma and a subscript, e.g., $u_{,x}$ means $\partial u/\partial x$ and $\Phi_{,yy}$ means $\partial^2\Phi/\partial y^2$.)

If the membrane stresses are expressed in terms of an Airy-type stress function ($\sigma_x = \Phi_{,yy}$, $\sigma_y = \Phi_{,xx}$, $\tau_{xy} = -\Phi_{,xy}$) and if Eqs. (1) are used, the von Kármán field equations of the large-deflection plate theory are obtained.[8] If the effect of inertia, normal to the middle surface of the plate, is included, the large-deflection plate equations in case of dynamic loading are

$$\nabla^4\Phi = E\left(w_{,xy}^2 - w_{,xx}w_{,yy}\right) \tag{2}$$

$$(D/h)\nabla^4 w = \Phi_{,xx}w_{,yy} - 2\Phi_{,xy}w_{,xy} + \Phi_{,yy}w_{,xx} - (\gamma/g)w_{,tt} \tag{3}$$

where Eq. (2) is the in-plane compatibility condition and Eq. (3) is the equation of transverse motion. Here h is the plate thickness, D is the flexural rigidity of the plate [$D = Eh^3/12(1-\nu^2)$, where E is the modulus of elasticity, and ν is the Poisson's ratio], γ is the specific weight of the plate, and g is the gravitational acceleration.

Choice of Deflection Function

As in the case of static loading, discussed by Kromm and Marguerre,[7] an infinitely long plate with simply supported edges, parallel to x axis, is considered (Fig. 1).

The deflection surface is represented by the following expression:

$$w(x, y, t) = f(t)\cos\frac{\pi y}{b}\cos\frac{\pi(x - my)}{s} \tag{4}$$

where s is the length of half-waves of the buckled plate and $m = \cot\alpha$ is the slope of nodal lines. The nodal lines are assumed to be approximately straight.

Equation (4) satisfies the boundary conditions with respect to the deflection ($w = 0$ for $y = -b/2$ and $y = b/2$ and also $w = 0$ along the nodal lines, for which $x - my = ns/2$, where $n = 1, 3, 5, \ldots$), but it does not satisfy the boundary conditions, regarding the vanishing of the bending moments along the longitudinal edges (i.e., $w_{,yy} \neq 0$ for $y = -b/2$) and $y = b/2$). However, an expression similar to that of Eq. (4) has been used for an approximate solution in the case of static loading.[7,9] This facilitates the analysis and the difference between the approximate and the exact values of the critical stress is relatively small (about 6.5%).[9]

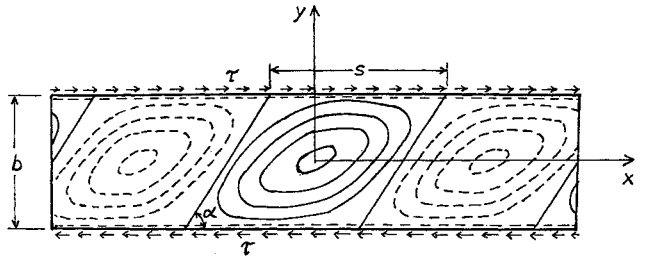

Fig. 1 Loading and deflection surface of the buckled plate.

Stress Function

If Eq. (4) is substituted into the compatibility condition, Eq. (2), we obtain

$$\nabla^4\Phi = -E\frac{\pi^4 f^2(t)}{2s^2b^2}\left[\cos\frac{2\pi y}{b} + \cos\frac{2\pi(x - my)}{s}\right] \tag{5}$$

A complementary solution of this nonhomogeneous differential equation is

$$\Phi(x, y, t) = -E\frac{f^2(t)}{32(1+m^2)}\left[\frac{1}{\beta^2}\cos\frac{2\pi(x - my)}{s} + \beta^2\cos\frac{2\pi y}{b}\right] - \tau(t)xy \tag{6}$$

where

$$\beta^2 = \frac{b^2}{s^2\sin^2\alpha} = \frac{b^2}{s^2}(1 + \cot^2\alpha) = \frac{b^2}{s^2}(1 + m^2) \tag{7}$$

Kromm and Marguerre[7] have proved that the contribution of the solution of the homogeneous equation $\nabla^4\Phi = 0$ can be neglected, and so the stress function remains in the form of Eq. (6). The second derivatives are

$$\sigma_x = \Phi_{,yy} = E\frac{\pi^2 f^2}{8b^2(1+m^2)}\left[\frac{m^2}{1+m^2}\cos\frac{2\pi(x - my)}{s} + \beta^2\cos\frac{2\pi y}{b}\right]$$
$$\sigma_y = \Phi_{,xx} = E\frac{\pi^2 f^2}{8b^2(1+m^2)^2}\cos\frac{2\pi(x - my)}{s} \tag{8}$$
$$\tau_{xy} = -\Phi_{,xy} = E\frac{\pi^2 f^2 m}{8b^2(1+m^2)^2}\cos\frac{2\pi(x - my)}{s} + \tau$$

With elementary calculations it can be proven that Eq. (6) satisfies the force boundary conditions,

$$\frac{1}{s}\int_{-0.5s}^{0.5s}\tau_{xy}\,dx = \tau, \quad \text{i.e.,} \quad \frac{1}{s}\int_{-0.5s}^{0.5s}(-\Phi_{,xy})\,dx = \tau$$
$$\frac{1}{s}\int_{-0.5s}^{0.5s}\sigma_y\,dx = 0, \quad \text{i.e.,} \quad \frac{1}{s}\int_{-0.5s}^{0.5s}\Phi_{,xx}\,dx = 0 \tag{9}$$

Solution of the Equation of Motion

On the basis of Eqs. (4) and (8) the derivatives of w and Φ are substituted in the equation of motion, Eq. (3):

$$\frac{D\pi^4 f}{h}\left\{\left[\left(\frac{1+m^2}{s^2} + \frac{1}{b^2}\right)^2 + \frac{4m^2}{b^2s^2}\right]\cos\frac{\pi y}{b}\cos\frac{\pi(x - my)}{s} + \frac{4}{bl}\left(\frac{1+m^2}{s^2} + \frac{1}{b^2}\right)\sin\frac{\pi y}{b}\sin\frac{\pi(x - my)}{s}\right\}$$
$$= 2\pi^2\tau f\left[\frac{m}{s^2}\cos\frac{\pi y}{b}\cos\frac{\pi(x - my)}{s} + \frac{1}{sb}\sin\frac{\pi y}{b}\sin\frac{\pi(x - my)}{s}\right] - \frac{\gamma}{g}\ddot{f}\cos\frac{\pi y}{b}\cos\frac{\pi(x - my)}{s}$$
$$- \frac{E\pi^4}{8b^2}f^3\left[\frac{1}{b^2(1+m^2)}\cos\frac{2\pi(x - my)}{s} + \frac{b^2}{s^4}\cos\frac{2\pi y}{b}\right]\cos\frac{\pi y}{b}\cos\frac{\pi(x - my)}{s} \tag{10}$$

An approximate solution will be found [because the coefficients in Eq. (10) involve functions of x and y]. First, the average values of the coefficients will be determined by using the Galerkin method. Each term in Eq. (10) is multiplied by $\cos(\pi y/b)\cos[\pi(x-my)/s]\,dx\,dy$ and then integrated over the middle surface of the plate (between $-s/2$ and $s/2$ in the x direction and between $-b/2$ and $b/2$ in the y direction). The result is a nonlinear second-order ordinary differential equation:

$$\ddot{f} + \frac{D\pi^4 g\beta^2}{hb^4\gamma(1+m^2)}\left[(1+m^2)\left(\beta^2+\frac{1}{\beta^2}\right)+6m^2+2\right]f - \frac{2\pi^2 gm\beta^2}{b^2\gamma(1+m^2)}\tau f + \frac{E\pi^4 g\beta^2}{16b^4\gamma(1+m^2)^2} \times \left(\beta^2+\frac{1}{\beta^2}\right)f^3 = 0 \tag{11}$$

To solve Eq. (11), we must first determine the parameters m and β. They depend on the external shear loading. The system of equations from which they can be determined can be derived from the system used by Kromm and Marguerre,[7] which is formed on the basis of the application of the principle of virtual displacements with respect to f, m, and β:

$$\tau m = \frac{\sigma_p}{2}(1+\beta^2) + E\frac{\pi^2 f^2}{16b^2(1+m^2)}\left[\beta^2+\frac{m^2}{\beta^2(1+m^2)}\right]$$

$$\beta^4 - 1 = \frac{E\pi^2 f^2}{4\sigma_p b^2(1+m^2)^2} \tag{12}$$

$$\frac{\tau}{m} = \frac{\sigma_p}{2}(3+\beta^2) - E\frac{\pi^2 f^2}{16b^2\beta^2(1+m^2)^2}$$

where $\sigma_p = 4\pi^2 D/(b^2 h)$.

The right-hand side of the second of Eqs. (12) is positive, or at the critical point ($f = 0$) it is zero, so that $\beta^4 - 1 \geq 0$, i.e., $\beta > 1$ in the postcritical range, and $\beta = 1$ at the critical point. First, f is eliminated and the system, depicted by Eqs. (12), is reduced to a system of two equations with two unknowns (m and β). It is solved numerically and the values of m and β^2 for various loading τ, greater or equal to τ_{cr} are obtained. The results for an infinitely long plate with width $b = 100$ cm, $E = 210{,}000$ MPa, and $\nu = 0.25$ are shown in Table 1.

Let us return to Eq. (11). The nature of the external loading must be specified. Let us consider for instance the case of $\tau = kt$ (i.e., τ increases linearly with time). Then Eq. (11) can be solved by means of a numerical method. The Runge–Kutta method in the form, given in Ref. 10, is chosen.

After $f(t)$ is found, it can be substituted into Eqs. (8) to determine the stresses.

From Eq. (11) one can derive the following:

1) The characteristic equation of the linear static buckling [by omitting the $\ddot{f}$ and f^3 terms in Eq. (11)] and, hence, the critical shear stress,

$$\tau_{cr} = \frac{D\pi^2}{2mhb^2}\left[(1+m^2)\left(\beta^2+\frac{1}{\beta^2}\right)+6m^2+2\right] \tag{13}$$

Substituting for m and β^2 in Eq. (13) their corresponding values from the first line of the first column in Table 1, we obtain the approximate smallest value for the critical shear stress[9]:

$$\tau_{cr} = 5.66D\pi^2/sb^2 \tag{14}$$

2) The large-deflection equation for the static postbuckling analysis [by omitting only the $\ddot{f}$ term in Eq. (11)]:

$$2m\left\{\frac{D\pi^2}{2mhb^2}\left[(1+m^2)\left(\beta^2+\frac{1}{\beta^2}\right)+6m^2+2\right]-\tau\right\}f + \frac{E\pi^2}{16b^2(1+m^2)}\left(\beta^2+\frac{1}{\beta^2}\right)f^3 = 0 \tag{15}$$

The coefficient in f^3 term is always positive. If $\tau > \tau_{cr}$, the coefficient of the f term is negative and a solution of Eq. (15) exists with $f > 0$.

Example

A dynamic buckling analysis of a long thin elastic plate (Fig. 1) is carried out on the basis of Eq. (11). For this plate, $b = 100$ cm, $h = 1$ cm, $E = 210{,}000$ MPa, $\nu = 0.25$, and $\gamma = 78.72$ kN/m^3 (steel). The static critical load is $\tau_{cr} = 104.2$ MPa [Eq. (14)]. The loading is in the form $\tau = kt$.

Three loading rates are considered: $k = 10\tau_{cr}$, $15\tau_{cr}$, and $20\tau_{cr}$. The time step is 0.001 s. Equation (11) is solved by the Runge–Kutta method and the values of f as a function of time t are obtained. The changes in m and β^2 with changes (increases) in τ (Table 1) are also taken into consideration. To obtain a solution with the Runge–Kutta method, different from the trivial one ($f = 0$), a very small value of f ($f = 0.001$ cm) is assumed at $t = 0$, and the initial conditions are $f = 0.001$ cm ≈ 0 and $\dot{f} = 0$ at $t = 0$.

Table 1 Values for m and β^2 in relation to τ/σ_p

τ/σ_p	m	β^2
1.414	0.7071	1.0000
1.5	0.7495	1.0758
1.6	0.7980	1.1520
1.7	0.8458	1.2202
1.8	0.8931	1.2814
1.9	0.9402	1.3335
2.0	0.9870	1.3815
2.1	1.0335	1.4269
2.2	1.0800	1.4660
2.3	1.1263	1.5030
2.4	1.1725	1.5370
2.5	1.2187	1.5675
2.6	1.2648	1.5961
2.7	1.3109	1.6221
2.8	1.3570	1.6459
2.9	1.4032	1.6669
3.0	1.4491	1.6889
3.1	1.4951	1.7084
3.2	1.5411	1.7266
3.3	1.5871	1.7435
3.4	1.6331	1.7593

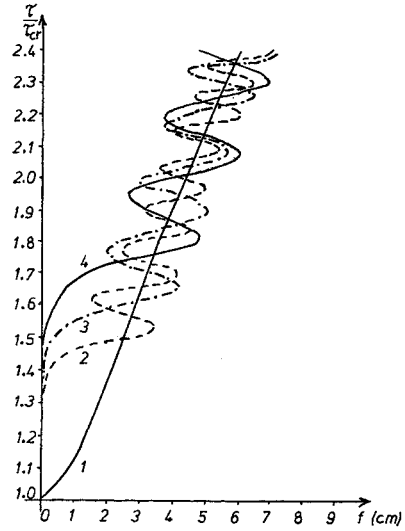

Fig. 2 Load-deflection curves for 1) static loading, 2) dynamic loading $k = 10\tau_{cr}$, 3) dynamic loading $k = 15\tau_{cr}$, and 4) dynamic loading $k = 20\tau_{cr}$.

The load-deflection curves for the three loading rates are given on Fig. 2, where also the curve of the static case [the nontrivial solution of Eq. (15)] is given for comparison.

The following features are observed on Fig. 2:

1) Instead of a definite point of instability (as it is in the static buckling analysis), there is a region of instability, where the slope of the response curve increases rapidly (for $k = 10\tau_{cr}$, when τ/τ_{cr} is between 1.40 and 1.50; for $k = 15\tau_{cr}$, when τ/τ_{cr} is between 1.55 and 1.66, and for $k = 20\tau_{cr}$, when τ/τ_{cr} is between 1.70 and 1.82).

2) The three load-deflection curves oscillate about the curve of the static solution.

3) The faster the loading rate, the greater the amplitude of oscillations and the smaller their frequency.

Besides, the stresses in case of a dynamic loading are higher than the corresponding static stresses, the factor being 1.75–1.80 for σ_x and 1.15–1.20 for τ_{xy}.

Conclusions

1) In case of a dynamic shear loading the slope of the load-deflection curve increases rapidly, which corresponds to the buckling of the plate, when the loading stress τ is greater than τ_{cr} (the critical stress for the case of static loading).

2) In the postbuckling range the load-deflection curve oscillates about the static load-deflection curve. This means that at definite moments the dynamic deflections are higher than the static ones, which leads to the fact that the dynamic stresses are higher than the corresponding static stresses. This must be taken into account during the design of a plate that is expected to be subjected to a dynamic loading.

3) The changes in m and β^2 with the increase of τ influence the results significantly and must be taken into account.

Acknowledgments

The author gratefully acknowledges the support of the U.S. Information Agency and the Council for International Exchange of Scholars in the form of a Fulbright grant, which made this work possible. The author would like to thank G. J. Simitses for his valuable advice, which was very important in the preparation of this Note.

References

[1]Simitses, G. J., *Dynamic Stability of Suddenly Loaded Structures*, Springer–Verlag, New York, 1990, pp. 5, 6.

[2]Ekstrom, R. E., "Dynamic Buckling of a Rectangular Orthotropic Plate," *AIAA Journal*, Vol. 11, No. 12, 1973, pp. 1655–1659.

[3]Zizicas, G. A., "Dynamic Buckling of Thin Elastic Plates," *Transactions of the American Society of Mechanical Engineers*, Vol. 74, No. 7, 1952, pp. 1257–1268.

[4]Ari Gur, J., Singer, J., and Weller, T., "Dynamic Buckling of Plates under Longitudinal Impact," *Israel Journal of Technology*, Vol. 19, 1981, pp. 57–64.

[5]Vol'mir, A. S., *Nonlinear Dynamics of Plates and Shells*, Publ. House Nauka, Moscow, 1972, pp. 228–231 (in Russian).

[6]Gerstein, M. S., "Buckling Analysis of Plates of a Ship's Hull," *Izvestiya VUZ, Mashinostroenie (Proceedings of the Institutions of Higher Education, Mechanical Engineering)*, No. 6, 1966, pp. 10–15 (in Russian).

[7]Kromm, A., and Marguerre, K., "Verhalten eines von Schub-und Druckkraeften beanspruchten Plattenstreifens oberhalb der Beulgrenze," *Luftfahrtforschung*, Vol. 14, 1937, pp. 627–639.

[8]Szillard, R., *Theory and Analysis of Plates*, Prentice–Hall, Englewood Cliffs, NJ, 1974, p. 342.

[9]Timoshenko, S. P., and Gere, J. M., *Theory of Elastic Stability*, McGraw–Hill, New York, 1961, pp. 382, 383.

[10]Korn, G., and Korn, T., *Mathematical Handbook for Scientists and Engineers*, McGraw–Hill, New York, 1968, p. 784.